Available online at www.sciencedirect.com
SCIENCE DIRECT
ELSEVIER
Nonlinear Analysis: Real World Applications 7 (2006) 12–24
Nonlinear Analysis
Real World Applications
www.elsevier.com/locate/na

Chaos prediction in the duffing-type system with friction using Melnikov's function

Jan Awrejcewicz*, Yuriy Pyryev

Department of Automatics and Biomechanics, Technical University of Łódź, 1/15 Stefanowskiego St., 90-924 Łódź, Poland

Received 14 February 2003; accepted 3 January 2005

Abstract

Nonlinear equations governing chaotic dynamics exhibited by a class of lumped mechanical systems with dry friction are analysed. It is shown that the obtained corresponding Melnikov's function can be simplified in some cases to yield analytical conditions for chaos occurrence. The analytical predictions are verified numerically.

Keywords: Melnikov's function; Chaos; Duffing-type system; Rotating shaft; Rigid bush; Friction

1. Introduction

Since nonlinear dynamical systems (NDS) may exhibit either regular or chaotic motions [1,2], one of the recent challenging tasks has been focused on their control. Such control can be realized, for instance, by applying an external kinematic excitation (perturbation). Although majority of the methods aiming at analysis and control of NDS are realized via numerical algorithms, an analytical treatment seems to be the most powerful and economical. One of the often applied approaches that allow one to calculate the distance between the homoclinic orbits, and yield the conditions of chaos occurrence in a nearly Hamiltonian system, is the Melnikov method [10] or the modified Melnikov theory [6–9]. This method has been widely applied to the analysis of smooth dynamical systems. Its successful application to analyze simple dynamical systems with friction has been illustrated only quite

* Corresponding author. Tel.:/fax: +48 42 6312225.
E-mail address: awrejcew@p.lodz.pl (J. Awrejcewicz).

1468-1218/$ - see front matter © 2005 Elsevier Ltd. All rights reserved.
doi:10.1016/j.nonrwa.2005.01.002

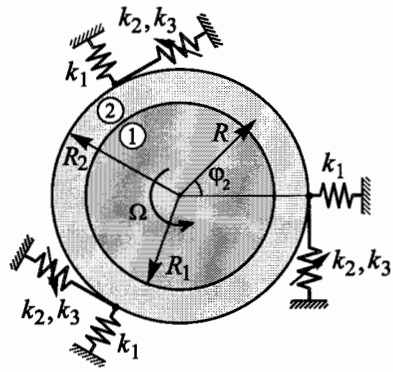

Fig. 1. Analyzed system (1—rotating shaft; 2—bush supported by springs).

recently [3]. This approach has even been extended to study of more complicated regular and chaotic stick–slip dynamics of a rotating shaft with a rigid bush in wear and heat transfer conditions [5]. The numerical experiments confirmed well an analytical prediction owing to analysis of a Melnikov's function.

In this work, the following mechanical system is analyzed (Fig. 1). An elastic and heat transferring shaft with radius R_1 is inserted into a bush. The bush is supported by massless springs. We assume that the bush is a perfectly rigid body and the "radial" ("tangent") springs are characterized by the stiffness coefficients k_1, and k_2, k_3 (Duffing type), respectively. Note that spring k_1 is initially stretched. The shaft rotates with such angular velocity $\Omega(t) = \Omega_* \omega_1(t)$ that centrifugal forces can be neglected. It is assumed that the angular velocity of the shaft is governed by equation $\omega_1 = \omega_* + \zeta_k \sin \omega' t$, where ζ_k is the non-dimensional amplitude of the kinematical external excitation. The next hypotheses follow: (a) heat transfer exchange between the bush and the shaft satisfies Newton's law; (b) the bush ideally transfers heat and, in the initial time instant, temperature of the environment changes with the law $T_0 h_T(t)$, where T_0 is a constant with units of temperature, and $h_T(t)$ is the known dimensionless time-varying function ($h_T(\tau) = 1 - \exp(-\delta\tau^2)$). Owing to the heat transfer, the rotating shaft starts to expand and touch the bush. Contrary to the purely numerical approaches to non-classical thermoelastic modeling of continuous systems addressed in the monograph [4], our attention is focused on obtaining an analytical threshold of chaos occurrence using the Melnikov method.

The classical model of dry friction between the shaft and the bush per length unit is governed by the function $F_t(V_r)$, where $V_r = \Omega R_1 - \dot{\varphi}_2 R_1$ characterizes the relative velocity of the shaft and the bush. B_2 is the bush inertial moment measured per length unit. In accordance with Amontos law, the friction force is governed by the equation $F_t = f(V_r)N(t)$, where $N(t)$ is the normal reaction and $f(V_r)$ is the kinematic friction coefficient.

2. Equations of motion

The analyzed mechanical system [5] with a periodic external kinematical excitation and the Duffing-type stiffness is shown in Fig. 1. One degree-of-freedom stick–slip oscillations

are governed by the following second-order non-dimensional form of the differential equation:

$$\ddot{\varphi}(\tau) - \varphi(\tau) + b\varphi^3(\tau) = \varepsilon F(\omega_1 - \dot{\varphi})p(\tau), \quad 0 < \tau < \infty. \tag{1}$$

The non-dimensional contact pressure is defined by the formula

$$p(\tau) = Bi\tilde{\omega}\int_0^\tau G_p(\tau - \xi)h_T(\xi)\,\mathrm{d}\xi, \quad G_p(\tau) = \sum_{m=1}^{\infty} \frac{4Bi}{Bi^2 + \mu_m^2}\,\mathrm{e}^{-\mu_m^2\tilde{\omega}\tau}, \tag{2}$$

where μ_m are the roots of the characteristic equation ($m = 1, 2, 3, \ldots$)

$$Bi\,J_0(\mu) - \mu J_1(\mu) = 0. \tag{3}$$

Friction against relative velocity dependence is approximated by the function

$$F(y) = F_0\,\mathrm{Sgn}(y) - \alpha y + \beta y^3, \quad \text{where } \mathrm{Sgn}(y) = \begin{cases} \{y/|y|\}, & \text{if } y \neq 0, \\ [-1, 1], & \text{if } y = 0. \end{cases} \tag{4}$$

The non-dimensional angular bush velocity is governed by the equation

$$\omega_1 = \omega_* + \zeta_k \sin\omega_0\tau, \tag{5}$$

where ζ_k is the non-dimensional amplitude of the kinematic external excitation.

The following non-dimensional quantities are introduced:

$$\tau = \frac{t}{t_*}, \quad \varphi(\tau) = \frac{\varphi_2(t_*\tau)}{\Omega_* t_*}, \quad b = \frac{k_3 R_2^4 t_*^4 \Omega_*^2}{B_2}, \quad \varepsilon = \frac{P_* t_* 2\pi R_1^2}{B_2\Omega_*}, \quad Bi = \frac{\alpha_T R_1}{\lambda_1},$$
$$\tilde{\omega} = \frac{t_* a_1}{R_1^2}, \quad \omega_0 = \omega' t_*, \quad F(\omega_1 - \dot{\varphi}) = f(R_1\Omega_*(\omega_1 - \dot{\varphi})),$$

where

$$t_* = \sqrt{B_2/(k_* R_2^2)}, \quad k_* = k_1(l_0/l_1 - 1)(1 + l_1/R_2) - k_2,$$
$$P_* = 2\alpha_1 E_1 T_0/(1 - 2\nu)$$

and E_1 is the elasticity modulus, ν the Poisson coefficient, l_0 the length of a non-stretched spring, l_1 the length of a stretched spring for $\varphi_2 = 0$, $k_* > 0$, α_1 the shaft thermal expansion coefficient, α_T the film heat transfer coefficient, a_1 thermal diffusivity, λ_1 is the thermal conduction of shaft.

3. The Melnikov's function

Introducing the new variables

$$x = \varphi, \quad y = \dot{\varphi}, \tag{6}$$

the equations of motion can be transformed (note that $p(\tau) \to 0.993$ for $\tau \to \infty$) into the following form:

$$\dot{x} = p_0(x, y) + \varepsilon p_1(x, y, \omega_0\tau, \varepsilon),$$
$$\dot{y} = q_0(x, y) + \varepsilon q_1(x, y, \omega_0\tau, \varepsilon), \tag{7}$$

where

$$p_0(x, y) = y, \quad p_1(x, y, \omega_0\tau, \varepsilon) = 0,$$
$$q_0(x, y) = x - bx^3, \quad q_1(x, y, \omega_0\tau, \varepsilon) = F(\omega_* + \zeta_k \sin\omega_0\tau - y). \tag{8}$$

For $\varepsilon = 0$, system (7) possesses the following homoclinic orbit of the form:

$$x_0(\tau) = \sqrt{\frac{2}{b}}\frac{1}{\cosh(\tau)}, \quad y_0(\tau) = -\sqrt{\frac{2}{b}}\frac{\sinh(\tau)}{\cosh^2(\tau)}. \tag{9}$$

For a sufficiently small parameter $0 < \varepsilon \ll 1$, the Melnikov's function is defined by the formula [3]

$$M(\tau_0) = \int_{-\infty}^{+\infty} (q_0 p_1 - q_1 p_0)|_{\substack{x=x_0(\tau-\tau_0)\\ y=y_0(\tau-\tau_0)}} \mathrm{d}\tau = -\int_{-\infty}^{+\infty} q_1 p_0|_{\substack{x=x_0(\tau-\tau_0)\\ y=y_0(\tau-\tau_0)}} \mathrm{d}\tau, \tag{10}$$

where $x_0(\tau)$, $y_0(\tau)$ is the solution of the non-disturbed system of equations ($\varepsilon = 0$), which corresponds to the homoclinic orbits, and τ_0 is the parameter that characterizes the positions of the point moving on this orbit. In accordance with Melnikov's theory, if the function $M(\tau_0)$ has simple zeros, then for a sufficiently small parameter ε, the motion governed by system (7) can be chaotic.

Introducing the change of variable $\tau - \tau_0 = t$, Melnikov's function reads as follows:

$$M(\tau_0) = -\int_{-\infty}^{+\infty} y_0(t)[F_0 \operatorname{Sgn}(\omega_r) - \alpha\omega_r + \beta\omega_r^3]\,\mathrm{d}t, \tag{11}$$

where the non-dimensional relative velocity has the form

$$\omega_r(t) = \omega_* + \zeta_k \sin(\omega_0(t + \tau_0)) - y_0(t). \tag{12}$$

The substitution of (9) and (12) into (11) yields Melnikov's function of the form

$$M(\tau_0) = I(\tau_0) + J(\tau_0), \tag{13}$$

where

$$\begin{aligned} J(\tau_0) &= 2C + 2\zeta_k\sqrt{A^2 + B^2}\sin(\omega_0\tau_0 + \varphi) \\ &\quad + 6\beta\zeta_k^2(I_{220}\cos^2\omega_0\tau_0 + I_{202}\sin^2\omega_0\tau_0 - 2\omega_* I_{111}\sin\omega\tau_0\cos\omega_0\tau_0) \\ &\quad + 2\beta\zeta_k^3(-I_{130}\cos^3\omega_0\tau_0 - 3I_{112}\sin^2\omega_0\tau_0\cos\omega_0\tau_0), \end{aligned}$$

$$A = (\alpha - 3\beta\omega_*^2)I_{110} - 3\beta I_{310}, \quad B = 6\beta\omega_* I_{201},$$
$$C = \beta I_{400} - (\alpha - 3\beta\omega_*^2)I_{200}, \quad \varphi = \arctan(A/B),$$
$$I_{njk} = \int_0^{\infty} [y_0(t)]^n [\sin(\omega_0 t)]^j [\cos(\omega_0 t)]^k\,\mathrm{d}t. \tag{14}$$

After the integration of Eq. (14) we obtain

$$I_{200} = \frac{2}{3b}, \quad I_{400} = \frac{8}{35b^2}, \quad I_{201} = \frac{\pi\omega_0(2 - \omega_0^2)}{6b\sinh(\pi\omega_0/2)},$$
$$I_{110} = -\frac{\pi\omega_0}{\sqrt{2b}\cosh(\pi\omega_0/2)},$$

$$I_{310} = \frac{\omega_0(11+10\omega_0^2-\omega_0^4)}{120b\sqrt{2b}}\left\{\psi\left(\frac{1-\mathrm{i}\omega_0}{4}\right)-\psi\left(\frac{3-\mathrm{i}\omega_0}{4}\right)\right.$$
$$\left.+\psi\left(\frac{1+\mathrm{i}\omega_0}{4}\right)-\psi\left(\frac{3+\mathrm{i}\omega_0}{4}\right)\right\},$$

$$I_{130} = -\frac{3\pi\omega_0}{8\sqrt{2b}}\left\{\cot\left(\frac{\pi(1-\mathrm{i}\omega_0)}{4}\right)+\cot\left(\frac{3\pi(1-\mathrm{i}\omega_0)}{4}\right)\right.$$
$$\left.-\cot\left(\frac{\pi(3-\mathrm{i}\omega_0)}{4}\right)-\cot\left(\frac{\pi(1-3\mathrm{i}\omega_0)}{4}\right)\right\},$$

$$I_{112} = \frac{\pi\omega_0\cosh(\pi\omega_0/2)}{\sqrt{2b}(1-2\cosh(\pi\omega_0))}, \quad I_{111} = -\frac{\pi\omega_0}{\sqrt{2b}\cosh(\pi\omega_0)},$$
$$I_{220} = \frac{\pi\omega_0(2\omega_0^2-1)+\sinh(\pi\omega_0)}{3b\sinh(\pi\omega_0)},$$

$$I_{202} = \frac{\pi\omega_0(1-2\omega_0^2)+\sinh(\pi\omega_0)}{3b\sinh(\pi\omega_0)}, \quad \Psi(z) = \frac{\Gamma'(z)}{\Gamma(z)},$$

where $\Psi(z)$ denotes the derivative of the natural logarithm of the function $\Gamma(z)$.

In (13), the term $I(\tau_0)$ is defined by the formula

$$I(\tau_0) = -F_0\int_{-\infty}^{+\infty} y_0(t)\,\mathrm{Sgn}(\omega_r)\,\mathrm{d}t = 2F_0\sqrt{\frac{2}{b}}\sum_m \frac{\mathrm{sgn}(\omega_r'(t_m))}{\cosh t_m}, \tag{15}$$

where t_m are the roots of the equation

$$\omega_r(t_m) = \omega_* + \zeta_k\sin(\omega_0(t_m+\tau_0)) - y_0(t_m) = 0, \tag{16}$$

whereas $\omega_r'(t) = \zeta_k\omega_0\cos(\omega_0(t+\tau_0)) - x_0(t) + bx_0^3(t)$.

4. Melnikov's function for large values of b

If Melnikov's function (13) changes its sign, then one may expect chaos. Observe that in our case, Melnikov's function has a rather complex structure and a direct theoretical analysis of it is not easy. Therefore, in this report, our considerations are limited to the analysis of the function $J(\tau_0)$ for large values of b and small values of ζ_k of the form:

$$J(\tau_0) = \left(-\frac{4}{3}(\alpha-3\beta\omega_*^2)+\frac{16}{35}\frac{\beta}{b}+O\left(\frac{1}{b^2}\right)\right)\frac{1}{b}$$
$$+\left[-\frac{\sqrt{2}\pi\omega_0(\alpha-3\beta\omega_*^2)}{\cosh(\pi\omega_0/2)}\cos(\omega_0\tau_0)-\frac{2\pi\omega_0\beta\omega_*(\omega_0^2-2)}{\sqrt{b}\sinh(\pi\omega_0/2)}\right.$$
$$\left.\times\sin(\omega_0\tau_0)+O\left(\frac{1}{b}\right)\right]\frac{1}{\sqrt{b}}\zeta_k+O(\zeta_k^2). \tag{17}$$

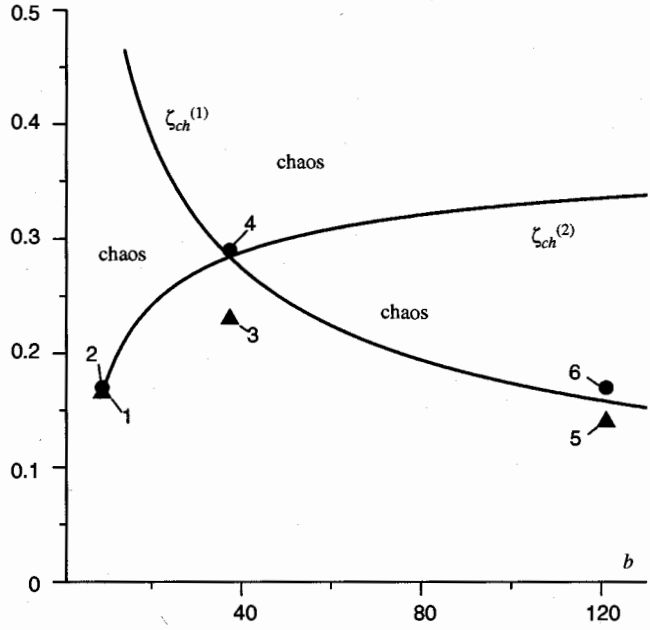

Fig. 2. Chaotic threshold in the (ζ_k, b) plane ($\varepsilon = 0.1$, $\omega_0 = 2$, $\omega_* = 0.4$, $F_0 = 0.3$, $\alpha = 0.3$, $\beta = 0.3$).

Eq. (17) yields the observation that the function $J(\tau_0)$ changes its sign (for large b and small ζ_k) when the following inequality holds:

$$\zeta_{ch}^{(1)} < \zeta_k \quad \text{where } \zeta_{ch}^{(1)} = \frac{4\cosh(\pi\omega_0/2)}{3\sqrt{2b}\pi\omega_0}. \tag{18}$$

Note that for large values of b and small values of ζ_k, we have $I(\tau_0) \equiv 0$, and the remaining terms of $J(\tau_0)$ in (13) are small. The value of the mentioned terms changes its sign when (18) holds. For a certain value of ζ_k, further referred to as ζ_{nz}, the value of integral $I(\tau_0)$ is not equal to zero, and starts to play a dominant role in $M(\tau_0)$. The function $M(\tau_0)$ begins to change sign, when $\zeta_k \geqslant \zeta_{nz}$ and when $I(\tau_0)$ is not equal to zero (the function $\omega_r(t)$ starts to change its sign). One may find the corresponding estimated value of the parameter ζ_k by using the following formula:

$$\zeta_{ch}^{(2)} < \zeta_k, \quad \zeta_{ch}^{(2)} \approx \zeta_{nz} = \omega_* - 1/\sqrt{2b}. \tag{19}$$

Using both formulas (18) and (19), the functions $\zeta_{ch}^{(i)}$, $i = 1, 2$ versus the parameter b are shown in Fig. 2. One may conclude that the region corresponding to chaos occurs above the curves.

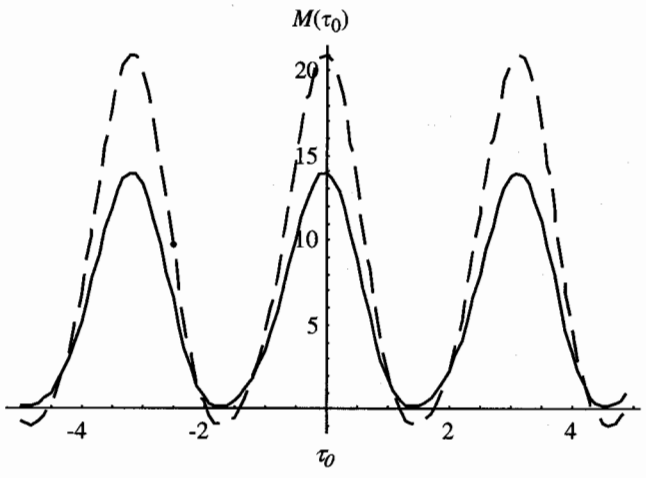

Fig. 3. Melnikov's function $M(\tau_0)$ versus parameter τ_0 for $\zeta_k = 3.2$ (continues curves) and for $\zeta_k = 3.81$ (dashed curves), and for $b = 1$.

5. Numerical results

In order to verify the analytical conditions of the chaotic oscillation occurrence, some numerical tests have been carried out. The following initial condition $x(0) = 0$, $y(0) = 0$ and the following parameters $\varepsilon = 0.1$, $\omega_0 = 2$, $\omega_* = 0.4$, $F_0 = 0.3$, $\alpha = 0.3$, $\beta = 0.3$ are fixed.

5.1. Arbitrary values of b

Formula (13) holds for any value of b. Numerically obtained Melnikov's function $M(\tau_0)$ is shown in Fig. 3 for $b = 1$.

Since Melnikov's function can change its sign (it has simple zeros) for $\xi_{ch} \approx 3.6$, chaos may occur according to Melnikov's theory. To confirm the analytical prediction, the bifurcational diagram $x(\zeta_k)$ has been constructed (projection of Poincaré section into the x-axis for $\zeta_k \in (0, 6)$ and $\zeta_k \in (3, 4)$). The obtained results are shown in Fig. 4.

Observe that for $\zeta_k < \omega_*$ ($\omega_* = 0.4$), the periodic motion occurs with the free frequency of the system, which undergoes changes as ζ_k increases. However, this motion vanishes when $\zeta_k \to \omega_*$. With the increase of the parameter ζ_k, period doubling occurs for $\xi_{ch} \approx 3.6$, and a bifurcation cascade leading to chaos follows.

In addition, for the same parameters fast fourier transform (FFT) of the process $x(\tau)$ for large values of $\tau \in (\tau_1, \tau_N)$ is reported. The computational results of the obtained power spectrum are shown in Fig. 5. The following relations are applied to estimate power spectra:

$$L(\omega) = 20 \log |X(\omega)|, \quad X(\omega) = X(\Delta_\omega m) = X_m,$$
$$\Delta_\omega = 2\pi/(\Delta_\tau N), \quad m = 1, 2, 3, \ldots, N,$$

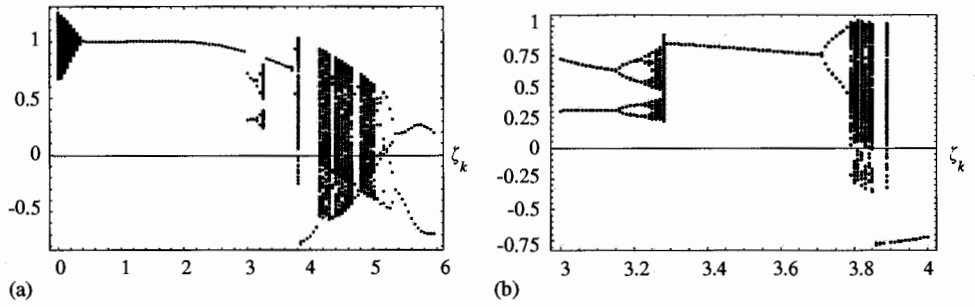

Fig. 4. Bifurcation diagrams using ζ_k as control parameter: (a) full diagram, (b) enlargement.

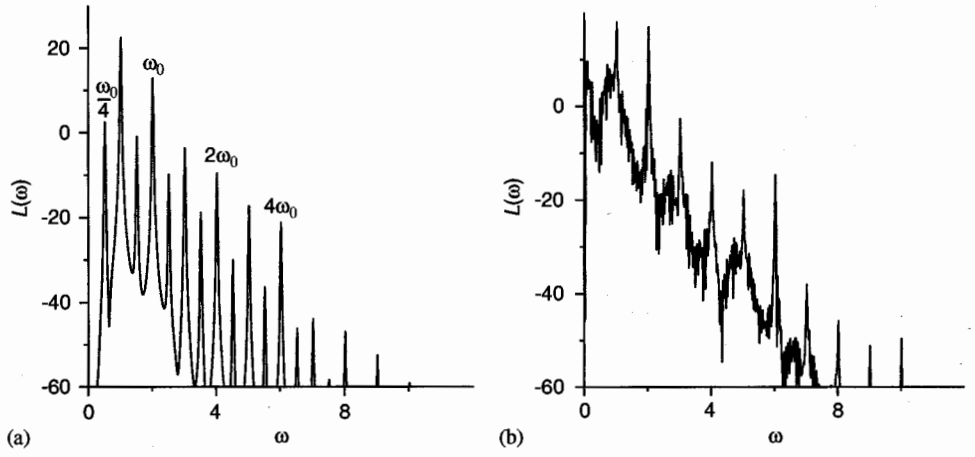

Fig. 5. Power spectrum: (a) $\zeta_k = 3.2$, (b) $\zeta_k = 3.81$.

$$X_m = \sum_{n=1}^{N} (x_n - x_0) e^{-2\pi i(n-1)(m-1)N}, \quad x_n = x(n\Delta_\tau), \quad n = 1, 2, 3, \ldots, N,$$

$$x_0 = \frac{1}{N} \sum_{n=1}^{N} x_n$$

and the following values are fixed during computations: $N = 4000$, $\Delta_\tau = 0.02$.

Observe that for $\zeta_k = 3.2$ the four periodic motion occurs, whereas for $\zeta_k = 3.81$, the motion is chaotic. The phase planes and Poincaré sections for ζ_k=3.2 (Fig. 6a) and ζ_k=3.81 (Fig. 6b) are shown. The points of Poincaré maps are obtained with respect to the period of kinematic excitation $2\pi/\omega_0$.

5.2. *Large values of b*

In general, for large values of the parameter b the values of ζ_k responsible for chaos occurrence are smaller in comparison with those of the parameter ω_*. As the numerical analysis

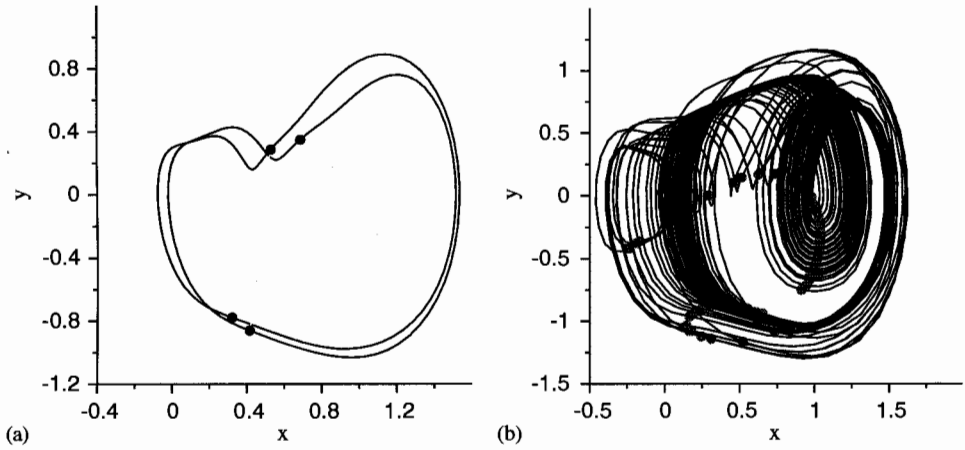

Fig. 6. Phase planes and Poincaré sections: (a) $\zeta_k = 3.2$, (b) $\zeta_k = 3.81$.

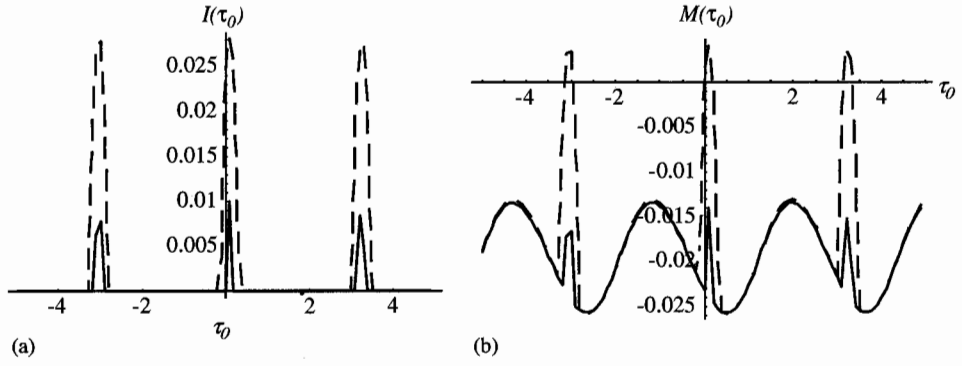

Fig. 7. Function $I(\tau_0)$ (a) and Melnikov's function $M(\tau_0)$ (b) versus the parameters τ_0 for $\zeta_k = 0.165$ (solid curves) and $\zeta_k = 0.17$ (dashed curves); $b = 9$.

shows, for $\zeta_k \in [0, \omega_*)$, the system motion is periodic with the free system frequency ω_d. For example, for fixed value of $b = 1$, the following values of ω_d are found: $\zeta_k = 0$ yields $\omega_d \approx 0.902$; $\zeta_k = 0.1$ yields $\omega_d \approx 0.805$; $\zeta_k = 0.2$ yields $\omega_d \approx 0.675$; $\zeta_k = 0.3$ yields $\omega_d \approx 1.43175$; $\zeta_k = 0.4$ yields $\omega_d = \omega_0 = 2$.

Numerical analysis of Melnikov's function is carried out for the parameters associated with the points 1–6 lying in the chaotic area (points 2, 4, 6) and out of chaos (points 1, 3, 5)—see Figs. 7, 9, 11. For $\zeta_k < \zeta_{nz}$, we have $I(\tau_0) = 0$. The obtained values of ζ_k give $\zeta_{nz} = 0.164$ (formula (19)) and $\zeta_{ch}^{(1)} = 0.58$ (formula (18)). Fig. 7 shows the dependence of the function $I(\tau_0)$ (a) and Melnikov's function $M(\tau_0)$ (b) versus the parameter τ_0 for points 1 ($b = 9$, $\zeta_k = 0.165$; solid curves) and 2 ($b = 9$, $\zeta_k = 0.17$; dashed curves) from Fig. 2. For the mentioned parameters, condition (18) is satisfied. Although for $\zeta_k = 0.165$

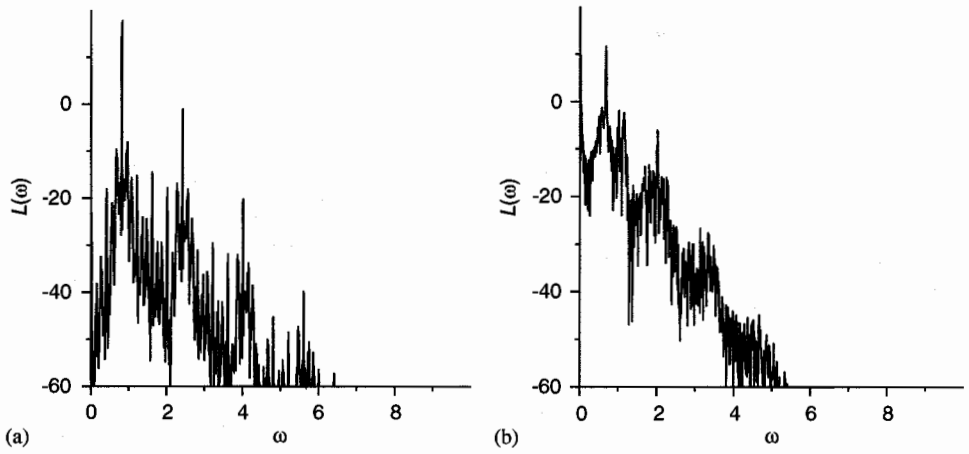

Fig. 8. Power spectrum for $b = 9$: (a) $\zeta_k = 0.1$, (b) $\zeta_k = 0.2$.

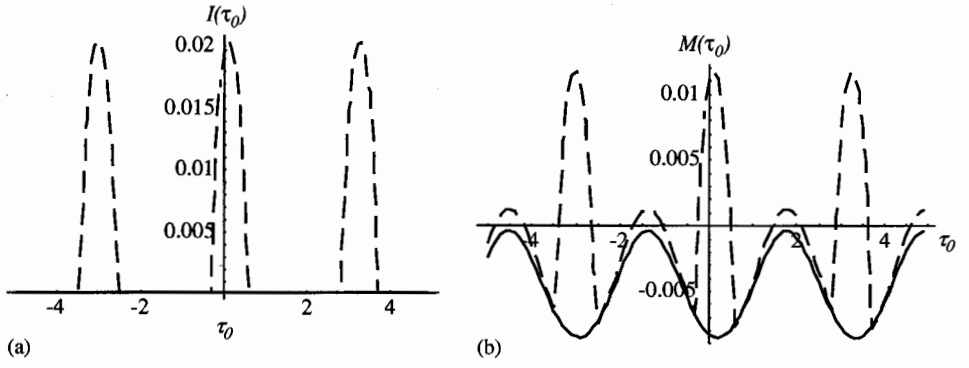

Fig. 9. $I(\tau_0)$ (a) and Melnikov's $M(\tau_0)$ (b) functions versus the parameter τ_0 for $\zeta_k = 0.23$ (solid curves) and for $\zeta_k = 0.30$ (dashed curves); $b = 37.41$.

the function $I(\tau_0)$ has non-zero values, the function $M(\tau_0)$ has not changed its sign yet. The numerical analysis shows that the function $M(\tau_0)$ changes its sign for $\zeta_{ch}^{(2)} \approx 0.168$. Hence, both obtained values of ζ_{nz} and $\zeta_{ch}^{(2)}$ are close to each other. The (numerical) analysis confirms the value of (19) used to obtain the parameter $\zeta_{ch}^{(2)}$ responsible for the occurrence of chaos according to Melnikov's rule.

Numerical analysis of Eq. (1) is carried out for the parameters in the vicinity of the points 1 and 2 (see Fig. 2). Fig. 8 illustrates the power spectra for the parameters $\zeta_k = 0.1$ (it corresponds to the point situated below point 1 and is associated with the quasi- periodic motion of the bush), and for $\zeta_k = 0.2$ (it corresponds to the point lying above point 2 and is associated with chaos).

Note that for $b = 37.41$ we have $\zeta_{ch}^{(1)} = \zeta_{ch}^{(2)}$ (see Fig. 2). Fig. 9 shows the $I(\tau_0)$ (a) and Melnikov's (b) $M(\tau_0)$ functions versus the parameter τ_0 for the parameters associated

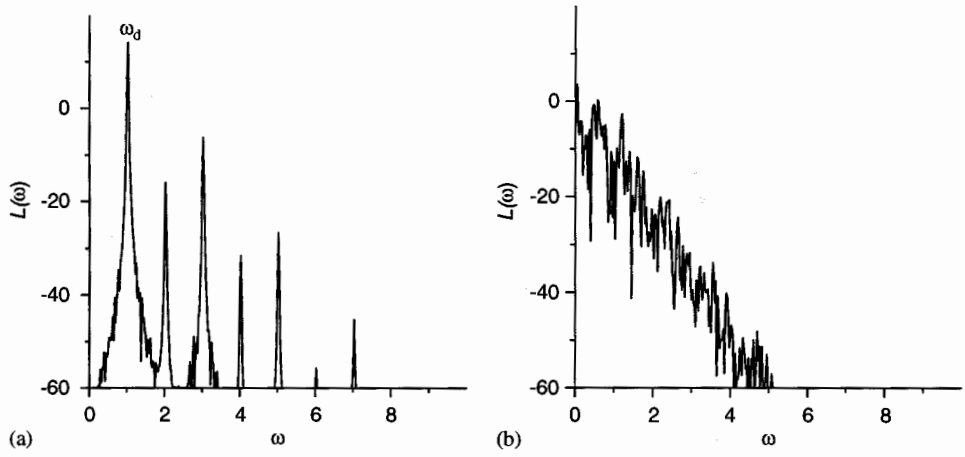

Fig. 10. Power spectra for $b = 37.41$: (a) $\zeta_k = 0.23$, (b) $\zeta_k = 0.29$.

with point 3 (see Fig. 2) ($b = 37.41$, $\zeta_k = 0.23$; solid curves) and with point 4 ($b = 37.41$, $\zeta_k = 0.30$; dashed curves). Although the function $I(\tau_0)$ is equal to zero, the function $M(\tau_0)$ still does not change its sign ($I(\tau_0) = 0$ for $\zeta_k < \zeta_{ch}^{(2)}$). It begins to change the sign for $\zeta_k = 0.30$. Therefore, the numerical tests confirm the values defined by Eqs. (18) and (19) and yielding the parameters $\zeta_{ch}^{(1)}$ and $\zeta_{ch}^{(2)}$ responsible for chaos occurrence, according to Melnikov's theory.

The numerical tests of Eq. (1) are performed for the parameter sets associated with the points 3 and 4 (Fig. 2). Fig. 10 presents the power spectra for the parameters $\zeta_k = 0.23$ (point 3 corresponds to the 2π-periodic bush motion) and $\zeta_k = 0.29$ (point 4 corresponds to chaotic motion). Chaotic behavior in the vicinity of the homoclinic orbits (9) is clearly visible for $\zeta_k = 0.29$.

In the next computational step, we have taken $b = 121$. Note that $I(\tau_0) = 0$ for $\zeta < \zeta_{ch}^{(2)}$. Formula (19) gives $\zeta_{ch}^{(2)} = 0.336$, whereas formula (18) yields $\zeta_{ch}^{(1)} = 0.158$. Fig. 11 presents the function $I(\tau_0)$ (a) and Melnikov's function $M(\tau_0)$ (b) versus τ_0 for the parameters associated with points 5 ($b = 121$, $\zeta_k = 0.14$; solid curves) and 6 ($b = 121$, $\zeta_k = 0.17$; dashed curves). In this case, $I(\tau_0) = 0$ for $\zeta_k = 0.14$, but the function $M(\tau_0)$ does not change its sign ($I(\tau_0) = 0$ for $\zeta_k < \zeta_{ch}^{(2)}$) (it starts to change it for $\zeta_k = 0.17$). Again numerical computations confirm the applied value of (18) to define the parameter $\zeta_{ch}^{(1)}$ responsible for the prediction of analytical chaos.

Finally, the numerical analysis of Eq. (1) is carried out for the parameters associated with points 5 and 6 in Fig. 2. For the parameters $\zeta_k = 0.1$ (the investigated point lies below the point 5 and corresponds to the periodic motion of the bush) and $\zeta_k = 0.17$ (point 6 corresponds to the narrow region of chaos), the associated power spectra are shown in Fig. 12.

Again, they confirm our analytical prediction.

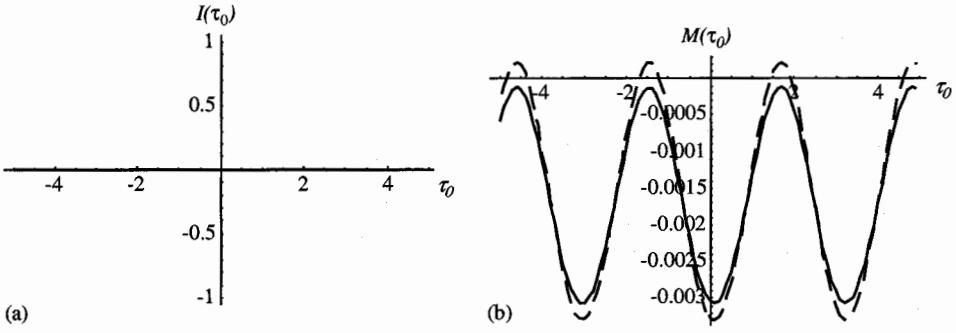

Fig. 11. $I(\tau_0)$ (a) and Melnikov's function $M(\tau_0)$ (b) versus the parameter τ_0 for $\zeta_k = 0.14$ (solid curves) and for $\zeta_k = 0.17$ (dashed curves); $b = 121$.

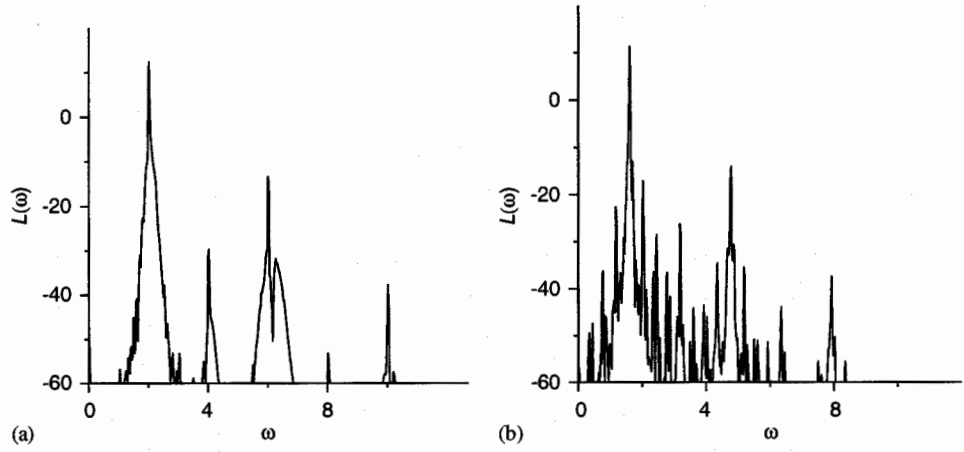

Fig. 12. Power spectra for $b = 121$: (a) $\zeta_k = 0.1$, (b) $\zeta_k = 0.17$.

6. Conclusions

It has been shown that for our investigated nonlinear system with friction the associated Melnikov's function can be constructed. As a result, one may control the nonlinear dynamics by analytical prediction of either regular or chaotic system state. For some parameter sets, the complicated analytical structure of the Melnikov's functions can be simplified to yield simple analytical conditions for the occurrence of chaos.

References

[1] J. Awrejcewicz, Bifurcation and Chaos in Simple Dynamical Systems, World Scientific, Singapore, 1989.
[2] J. Awrejcewicz, Bifurcation and Chaos in Coupled Oscillators, World Scientific, Singapore, 1991.

[3] J. Awrejcewicz, M.M. Holicke, Melnikov's method and stick–slip chaotic oscillations in very weakly forced mechanical systems, Int. J. Bifurc. Chaos 9 (1999) 505–518.
[4] J. Awrejcewicz, V.A. Krysko, Nonclassical Thermoelastic Problems in Nonlinear Dynamics of Shells, Springer, Berlin, 2003.
[5] J. Awrejcewicz, Yu. Pyryev, Thermoelastic contact of a rotating shaft with a rigid bush in conditions of bush wear and stick–slip movements, Int. J. Eng. Sci. 40 (2002) 1113–1130.
[6] M. Belhaq, M. Houssni, Suppression of chaos in averaged oscillator driven by external and parametric excitations, Chaos Solitons Fract. 11 (2003) 1237–1246.
[7] Q. Cao, K. Djidjeli, W.G. Price, E.H. Twizell, Periodic and chaotic behaviour in a reduced form of the perturbed generalized Korteweg-de Vries and Kadomtsev-Petviashvili equations, Physica D 125 (1999) 201–221.
[8] S. Lenci, G. Rega, Higher-order Melnikov functions for single-dof mechanical oscillators: theoretical treatment and applications, Math. Problems Eng. 2 (2004) 145–168.
[9] B. Massimiliano Berti, C. Carminati, Chaotic dynamics for perturbations of infinite-dimensional Hamiltonian systems, Nonlinear Anal. 48 (2002) 481–504.
[10] V.K. Melnikov, On the stability of the center for time periodic perturbations, Trans. Moscow Math. Soc. 12 (1963) 1–57.